



## **A smartphone biosensor based on analysing structural colour of porous silicon**

Journal:	<i>Analyst</i>
Manuscript ID	AN-ART-01-2019-000022.R1
Article Type:	Paper
Date Submitted by the Author:	14-Apr-2019
Complete List of Authors:	Cao, Tengfei; Vanderbilt University, Zhao, Yiliang; Vanderbilt University, Nattoo, Crystal; University of Miami College of Engineering, Layouni, Rabeb; Vanderbilt University, Chemical and Molecular Engineering Weiss, Sharon M.; Vanderbilt University, Electrical Eng. & Comp. Sci.



## A smartphone biosensor based on analysing structural colour of porous silicon

Tengfei Cao,<sup>a</sup> Yiliang Zhao,<sup>a</sup> Crystal A. Nattoo,<sup>b,c</sup> Rabeb Layouni,<sup>d</sup> and Sharon M. Weiss<sup>\*a,c</sup>

Received 00th January 20xx,  
Accepted 00th January 20xx

DOI: 10.1039/x0xx00000x

[www.rsc.org/](http://www.rsc.org/)

We report a smartphone compatible, low-cost porous silicon biosensor, which correlates the structural colour of a porous silicon microcavity (PSiM) to spectral intensity. Molecules captured in the PSiM cause a colour change that can be quantified through image analysis. Minimal external accessories are employed. Spectrometer measurements of the PSiM reflectance spectrum shifts are carried out concurrently with the smartphone measurements to benchmark the accuracy of the smartphone biosensor. We estimate that the smartphone biosensor supports an equivalent accuracy of 0.33 nm for the detection of colour changes corresponding to spectral shifts of the PSiM. Biosensing functionality is demonstrated using a biotin-streptavidin assay with an estimated detection limit of 500 nM. The PSiM-smartphone biosensor is a promising platform for label-free point of care diagnostics.

### 1. Introduction

Point-of-care (POC) diagnostics is a fast-growing sector in the diagnostics market due to the convenience and low cost of POC measurements.<sup>1</sup> Biosensors are the crucial elements of POC diagnostics, which transform biomolecular or medical information into easily understandable readouts. Current mainstream sensing technologies include enzyme-linked immunosorbent assay (ELISA),<sup>2,3</sup> mass spectrometry (MS),<sup>4</sup> surface plasmon resonance (SPR),<sup>5,6</sup> polymerase chain reaction (PCR),<sup>7</sup> and electrochemical immunoassays.<sup>8,9</sup> These technologies have achieved high sensitivity and accuracy, and are being widely used in hospitals and other laboratories. However, tests run using these mainstream sensing technologies generally require high-cost instrumentation, strict sample preparation procedures, and well-trained personnel, which restrict their usage for POC applications. There have been many efforts to create portable sensing technologies for POC diagnostics, including glucose meters,<sup>10</sup> paper-based test strips,<sup>11,12</sup> and lab on chip devices.<sup>13</sup> These sensors have the advantage of low cost and convenience, but are generally designed for a single purpose instead of multi-parameter testing. Moreover, the data processing capabilities of these sensors are usually basic and not intended for more complicated detection and analysis tasks. Over the past few

years, smartphones have emerged as a promising host platform for POC diagnostics systems due to their ubiquitous availability and advanced computational capabilities.<sup>14</sup> Smartphones are often integrated with high-quality sensors that can be repurposed to facilitate sensing applications, and internet connectivity enables further extension of their capabilities. Significant advances in the area of smartphone sensing have been reported for smartphone microscopy<sup>15,16</sup>; colorimetric test strip,<sup>17,18</sup> lateral flow assay,<sup>19,20</sup> and ELISA readers;<sup>21</sup> SPR sensors;<sup>22,23</sup> spectrometers;<sup>24,25</sup> and fluorimeters.<sup>26</sup> In many cases, the reported smartphone devices dramatically reduce the cost factor while maintaining comparable performance to benchtop instruments. For example, based on a smartphone and external, disposable optical system, Filippini et al. demonstrated an angle-resolved SPR sensor that measured a refractive index change of  $2 \times 10^{-6}$  RIU.<sup>22</sup> By adding external illumination and a diffraction grating, Cunningham et al. reported a smartphone spectrometer with extremely high accuracy, and a fluorescence-based spectrophotometer showing comparable performance to conventional laboratory fluorimeters.<sup>24,26</sup> Ozcan et al. reported a smartphone microplate reader for ELISA that demonstrated >99% accuracy in screening for several diseases.<sup>21</sup>

In this paper, we present a new implementation for a cost-effective, sensitive smartphone biosensor that requires only a bandpass filter and a 3D printed box, and leverages the advantages of the high surface area sensor material, porous silicon, for the test chip. The biosensing system works by detecting the structural colour change of a porous silicon microcavity (PSiM) that results when target molecules are captured in the pores of the PSiM. This sensing approach is different from traditional colorimetric approaches that require, for example, an enzymatic reaction, fluorescent species, or nanoparticle aggregation to cause a colour change.<sup>27,28</sup> While

<sup>a</sup> Interdisciplinary Graduate Program in Materials Science, Vanderbilt University, Nashville, TN 37235, USA.

<sup>b</sup> Department of Electrical and Computer Engineering, University of Miami, Coral Gables, FL 33146, USA.

<sup>c</sup> Department of Electrical Engineering and Computer Science, Vanderbilt University, Nashville, TN 37235, USA. E-mail: sharon.weiss@vanderbilt.edu.

<sup>d</sup> Department of Chemical and Biomolecular Engineering, Vanderbilt University, Nashville, TN 37235, USA.

\*Electronic Supplementary Information (ESI) available. See DOI: 10.1039/x0xx00000x

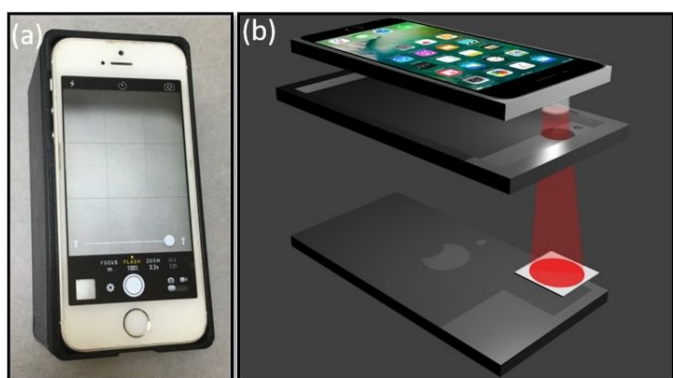


Figure 1 Smartphone biosensing system. (a) Photograph showing smartphone situated in 3D printed box. (b) Schematic illustration in a cut-away view showing, from top to bottom, the smartphone with red bandpass filter inserted in front of the smartphone LED flash, the top of the 3D printed box, the PSiM positioned below the smartphone camera, and the bottom of the 3D printed box.

label-free porous silicon optical biosensors have been previously reported for high detection sensitivity of a variety of analytes, cost-effective fabrication, compatibility with many surface chemistries, and molecular detection in complex media, their operation relies on lamps or lasers for the light source and benchtop spectrometers or power meters for the detector.<sup>29,30</sup> By using the built-in LED flash of a smartphone as the light source and the smartphone camera as the photon detector, a suitably designed label-free porous silicon sensor can operate without a benchtop measurement system. Moreover, a porous silicon smartphone sensor does not require external lenses or gratings, as is the case for many other smartphone biosensors. Here, we demonstrate that a label-free PSiM smartphone sensing system can operate with an equivalent accuracy of 0.33 nm and an estimated detection limit of 500 nM based on a biotin-streptavidin assay. We note that the spectrometer measurements reported in the paper are necessary only for characterizing the intrinsic properties of the system, and are not necessary for quantifying molecular detection events. Calibration between the light intensity and concentration of target molecules is the only prerequisite for quantitative detection applications.

## 2. Materials and methods

### Materials

All chemicals were analytical grade and used without further purification. Single side polished, boron doped p-type silicon wafers ((100), 0.01–0.02  $\Omega$  cm, 500–550  $\mu$ m) were purchased from Pure Wafer, WRS Materials Company. N-Hydroxysuccinimide (NHS) and 10-Undecenoic acid were purchased from Alfa Aesar. N-(3-Dimethylaminopropyl)-N'-ethylcarbodiimide hydrochloride (EDC), EZ-Link Amine-PEG2-Biotin, sulfo-NHS-biotin, streptavidin and ethanol were all purchased from Thermo Fisher Scientific. Hydrofluoric acid (HF) was purchased from Acros Organics. Deionized (DI) water ( $\sim$ 15 M $\Omega$ -cm) was used as a solvent for all experiments except where noted otherwise.

### Reflectance measurements

A Newport Oriel 6000 Q Series Lamp and fibre-coupled Ocean Optics USB-4000 spectrometer were used for reflectance measurements over a sample area of approximately 1 mm<sup>2</sup> and wavelength range of 400 – 900 nm. Spectral shifts to longer wavelengths (i.e., redshift) indicate that molecules have attached inside the PSiMs while spectral shifts to shorter wavelengths (i.e., blueshift) indicate that material has been removed from the PSiMs.

### Smartphone measurements

An iPhone SE, model A1662, was used to carry out quantitative measurements of the colour of the PSiMs. Broadband white light was emitted from the smartphone LED and transmitted through a Thorlabs bandpass filter (centre wavelength  $\lambda_0$  = 606.5 nm; full-width-at-half-maximum (FWHM) = 10 nm; see Fig. 2c) before reflecting off the porous silicon sample. The reflected light was collected by the smartphone camera. We note that it should be possible to replace the Thorlabs bandpass filter with a free-standing porous silicon bandpass filter, if desired. To achieve a more uniform illumination, we attached a piece of white paper to the phone in front of the LED to diffuse the light, and we also added a small piece of black tape on the back side of the filter fixture to block the brightest spot of light emitted from the LED. A custom 3D printed box was fabricated and used to hold the smartphone, filter, and PSiM in fixed positions during all measurements (Figure 1). A camera app developed by KendiTech was used to control the focus, flash, zoom, ISO, speed, exposure value and white balance of the smartphone camera. Videos clips of approximately 1 min were recorded instead of taking individual pictures for better accuracy and reproducibility. The videos were uploaded to a desktop computer, and a MatLab code was used to convert the videos into arrays of time sequenced intensity values. Each video was treated as a series of RGB images, and the data comprising one RGB image was exported to three matrices in MatLab that contain the intensities measured by the red (R), green (G), and blue (B) pixels, respectively, in the camera imaging sensor. In this work, we only use the R-values in our calculations because the bandpass filter restricts the incident light to red wavelengths. Detailed procedures for the smartphone measurements are provided in ESI†. We anticipate that the computations carried out on the desktop computer in this work could also be carried out directly on the phone using an appropriately designed app or through a cloud computing approach.

### Fabrication and surface modification of PSiMs

PSiMs were prepared by anodic etching of p-type silicon wafers in 15% HF in ethanol. Note that HF is an extremely dangerous chemical and should be handled with the utmost caution. First, a sacrificial layer was etched with a current density of 70 mA·cm<sup>-2</sup> for 100 s and then dissolved in 1 M NaOH solution. The sample was then thoroughly cleaned with ethanol and DI water. Next, alternating current densities of 80 mA·cm<sup>-2</sup> for 3.1 s and

60 mA·cm<sup>-2</sup> for 3.2 s were applied in the following manner to form the optical microcavity structure where H and L designate the higher and lower current density, respectively, and the layers are designed to have an optical thickness corresponding to one quarter of the resonance wavelength: (HL)<sup>7</sup>(HH)(LH)<sup>7</sup>. Following anodization, freshly prepared PSiMs were modified by thermal hydrosilylation. Undecenoic acid was added to a Schlenk flask and underwent three freeze-pump-thaw cycles in order to remove oxygen. Prior to the reaction, the sample was dipped into 2.5% HF solution for 90 seconds to remove the native oxide. The sample was then transferred to the Schlenk flask under a constant nitrogen flow. The flask was then immersed in an oil bath at 120 °C and the reaction proceeded over 5 hours. Finally, the sample was rinsed thoroughly with tetrahydrofuran, dichloromethane and ethanol, and dried under a nitrogen stream.

#### APTES measurement for sensor benchmarking

To benchmark the performance of the PSiM-smartphone sensing system, we carried out an experiment to determine the relationship between spectral changes measured by an Ocean Optics spectrometer and colour changes measured by the smartphone camera (as described in the next section). A stepwise change in the refractive index of the PSiM was achieved by multiple exposures of the sample to a 0.1% (v/v) solution of APTES in ethanol. For each exposure, 100 μL of the APTES solution was drop cast on the PSiM and incubated for 30 s, followed by gentle blowing with nitrogen gas to remove excess solution from the surface. The PSiM was measured with

the spectrometer after each APTES exposure to quantify the spectral shift. The PSiM was then measured three times by the smartphone to quantify the colour change. APTES is a commonly used chemical for surface modification, which is known to form multilayer structures.<sup>31</sup> APTES attachment can therefore lead to large spectral shifts of the PSiM, which is necessary for the benchmarking of the sensor performance. We note that other molecules could have also been used and would have resulted in the same correlation between spectrometer and smartphone measurements for the given PSiM.

#### Biotin—streptavidin sensing

To achieve biotin functionalization, the hydrosilanized PSiM was first soaked in 1 mL 0.1 M NHS aqueous solution followed by 1 mL 0.4 M EDC. The reaction proceeded in a dark environment and gentle shaking was applied every 5 min. After 30 min, the sample was cleaned in DI water and rinsed in ethanol for 15 min. Next, the sample was soaked in 1 mg·mL<sup>-1</sup> amine-PEG-Biotin solution for 30 min. Finally, a 80 μL aliquot of 0.5 μM streptavidin mixed with 10 μL of ethanol was pipetted onto the PSiM sample and incubated for 60 min. The ethanol is added to reduce the surface tension between the water and hydrosilanized surface. The sample was then cleaned with DI water and ethanol three times, soaked in ethanol for 5 min and gently blown dry under nitrogen gas. After each step in the sensing experiment, the PSiM was measured with both the spectrometer and smartphone. The PSiM was subsequently exposed to 1 μM, 2 μM and 4 μM concentrations of streptavidin in water following the same procedures. We note that the

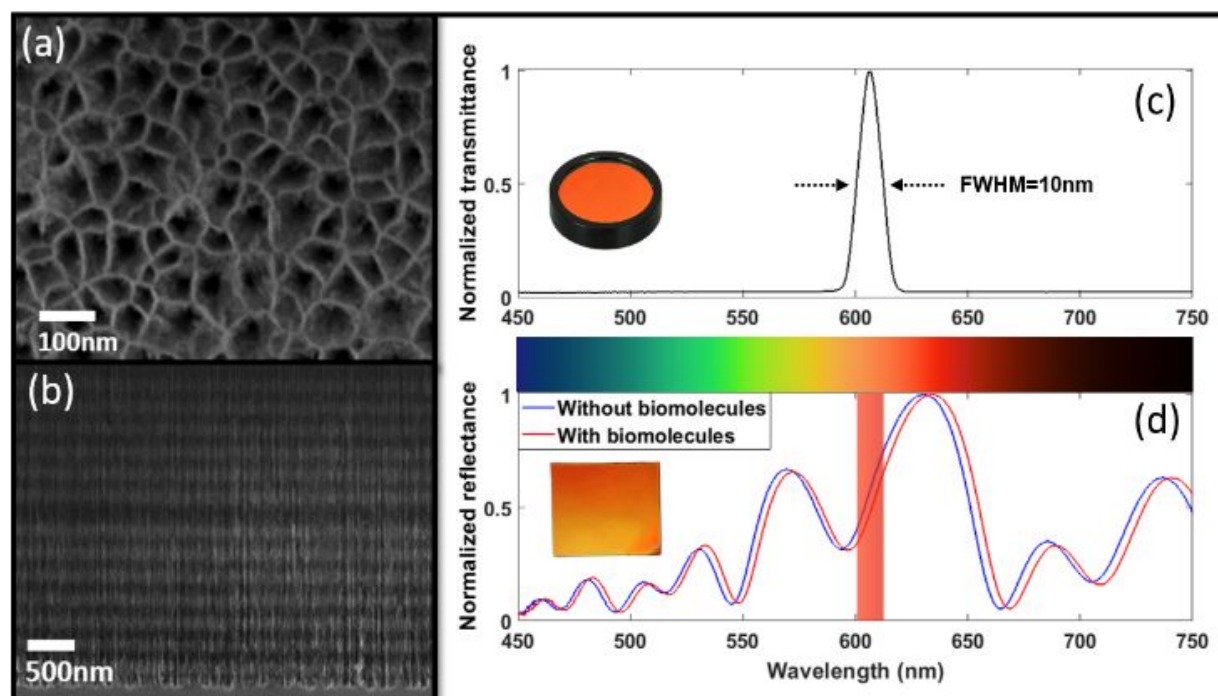


Figure 2 SEM images of PSiM in (a) top view and (b) cross-sectional view. (c) The normalized spectral intensity of the smartphone LED light after passing through the bandpass filter (shown in the inset), which is centred at 606.5 nm in this work. (d) Typical reflectance spectra of PSiM. The blue and red curves are the reflectance spectra before and after adding biomolecules, respectively. The red shaded region indicates the position of the filter. A photograph of a PSiM sample is shown in the inset.

magnitude of the change in the spectral and intensity responses of the PSiM sensor are dependent on the incubation time of the target molecule. Based on prior work, we anticipate a measurable signal change could be achieved after a few minutes of exposure to the streptavidin solution;<sup>32</sup> however, the magnitude of the signal change would be much less than what we report here for a 60 min exposure and would therefore also affect the limit of detection. To verify that there is no non-specific attachment of streptavidin on the PSiM, a control experiment was carried out. A 80  $\mu\text{L}$  volume of 1  $\mu\text{M}$  sulfo-NHS-Biotin (1 mM) blocked streptavidin solution mixed with 10  $\mu\text{L}$  ethanol was drop cast onto a biotinylated sample, incubated for 60 min, then rinsed with water and ethanol three times, and blown dry with nitrogen before measurement.

### 3. Results and discussion

#### Porous silicon microcavity characterization

Scanning electron microscopy (SEM) images of a PSiM are shown in Fig. 2. Based on image analysis, the estimated average pore size, porosity, and thickness of the porous silicon layers fabricated with the higher current density are  $\sim 60$  nm, 82%, and 120 nm, respectively. The estimated average pore size, porosity, and thickness of the porous silicon layers fabricated with the lower current density are  $\sim 40$  nm, 75%, and 97 nm, respectively. A reflectance spectrum of the microcavity is shown in Fig. 2d. The resonance wavelength is near 600 nm and the peak of the high reflectance band on the long wavelength side of the resonance is near 630 nm. The refractive index sensitivity of the PSiM is determined to be near 350 nm/RIU as detailed in the ESI<sup>†</sup>. In this work, the most important design criterion is having a sharp spectral feature near the centre wavelength of the bandpass filter, as discussed in the next subsection.

#### Basic principle of smartphone biosensor

The smartphone is able to facilitate label-free optical biosensing with porous silicon by detecting the structural colour change of a PSiM upon a specific bio-recognition event. When molecules attach to the pore walls, the effective refractive index of the porous silicon increases and results in a redshift of the reflectance spectrum, as illustrated in Fig. 2d for a PSiM. This spectral change is commonly detected by a spectrometer that measures reflection or transmission spectra over a wavelength range of hundreds of nanometres. However, it is not always necessary to measure broadband spectra to identify a molecular detection event. Instead, molecular detection events in PSiMs can be identified by appropriately analysing colour changes using a smartphone. Figure 2d conceptually illustrates how a spectral shift resulting from a molecular binding event can also be detected as a colour change. The rectangular shaded region represents the approximate spectral bandwidth of light that reaches the smartphone camera due to the presence of the bandpass filter. When molecules are added to the PSiM, the resulting spectral shift leads to a change in the integrated intensity of light measured by the smartphone camera. In

Fig. 2d, with the bandpass filter designed to overlap with the long wavelength edge of the resonance of the PSiM, the addition of molecules leads to a decrease in the intensity of light measured by the smartphone since the intensity of reflected light at each wavelength within the measurement window decreases with molecular attachment. The steeper the reflectance spectrum is within the measurement window, the larger the change in light intensity measured by the smartphone camera will be for a given reflectance spectrum shift (i.e., given refractive index change of the PSiM due to molecular infiltration). Hence, other PSi thin film designs, such as edge filters, may lead to improved sensing performance compared to the PSiM. Nevertheless, in this work, the PSiM provides a convenient platform to compare smartphone and spectrometer measurements while yielding good detection sensitivity. A comparison curve can be established that directly relates changes in spectral properties typically measured by a spectrometer with light intensity measured by the smartphone camera. This correlation is only necessary to benchmark the sensitivity of the smartphone detection platform in comparison to a traditional spectrometer. We note that the dynamic range of measurement using the smartphone detection platform, which is directly related to the maximum number or concentration of molecules that can be quantified by the smartphone detection platform, is limited by the wavelength range over which there is a monotonic change in reflectance intensity.

#### Engineering challenges with smartphone/PSiM biosensor

There are several engineering challenges when assembling the system in the box that must be overcome to realize a robust biosensor that may be suitable for POC diagnostic applications. Although we only introduce the engineering challenges here, we believe sufficient process development would enable mitigation of the negative consequences of the current challenges. First, the light emitted from the smartphone LED does not have uniform spatial intensity. Most of the light is concentrated in the center of the emission region, which can lead to saturation of the smartphone image sensors. As a simple approach to improve the illumination uniformity, we attached a piece of white paper to the outside of the smartphone LED to diffuse the emitted light, and we also used a piece of black scotch tape to block the region of highest intensity emitted light, as discussed in Section 2 (Smartphone measurements). More sophisticated light management approaches would be necessary to achieve a highly uniform intensity of incident light on the PSiM sample. A second challenge is the nonuniformity of the porous silicon sample itself. Slight differences in the local thicknesses of the porous silicon layers comprising the PSiM lead to changes in the measured reflectance spectrum across the sample. For example, the microcavity resonance wavelength, and likewise the high reflectance peak position, can vary by as much as 10 nm when different spots on the same PSiM sample are measured. Moreover, sample to sample variation in the shape and position of the reflectance band edge would introduce error into the quantification of the sensing

measurements. Optimizing the electrochemical fabrication conditions, including control of the temperature and humidity conditions and electrode design, can lead to significantly improved porous silicon uniformity. Together, the nonuniform illumination and nonuniformity of the porous silicon can lead to significant changes in the measured light intensity by the smartphone camera when there is any change in the smartphone position with respect to the PSiM sample position. Figure S3 in ESI<sup>†</sup> shows a typical smartphone camera image of the PSiM and the associated R-value contour map of the image, revealing that the R-value varies significantly across the PSiM. Accordingly, a third engineering challenge is mechanical vibrations that cause displacement between the positions of the smartphone and PSiM sample, which lead to unwanted changes in measured light intensity that are not related to molecular binding. An improved 3D printed box design could enable the smartphone and PSiM sample to be fixed more robustly in place. Moreover, in the current implementation of the PSiM-smartphone biosensor, the PSiM sample is removed from the 3D printed box each time a new molecule is exposed to the sample. The measured intensity variation caused by removing and reloading the sample is shown in ESI<sup>†</sup>. In future designs, improved methods of fluidic handling could eliminate the need to remove the sample from the box. In the present work, to mitigate error arising from smartphone-PSiM relative displacement, the area enclosed by a constant R-value contour curve is chosen to represent the effective light intensity value measured by the smartphone. This  $R \geq R_0$  criterion, where  $R_0 = 30$  in this work, automatically defines the boundaries of the analytical region under consideration and enables the best resilience to mechanical vibration. The effective light intensity is calculated by summing the R values of the pixels within the area enclosed by the  $R = 30$  contour curve. An average effective light intensity value is reported for each 1 min video measurement based on the average value calculated from approximately 500 images from the video. After each smartphone measurement of the PSiM, a bare silicon sample is measured as a control sample to account for any changes in the smartphone LED intensity over time. The average effective light intensity of the sample under test is normalized with respect to the average effective light intensity of the control sample, and is denoted as the relative intensity. In future work, the control sample could be measured at the same time as the test sample by imaging a region that contains both the PSiM and an unetched region of bare silicon.

#### Smartphone biosensor benchmarking with APTES infiltration

To benchmark the performance of the smartphone biosensor with a traditional spectrometer, a PSiM was exposed to 0.1% APTES in ethanol and subsequently blown dry and measured by both the smartphone and spectrometer. As shown in Figure 3a, the reflectance spectrum measured by the spectrometer redshifts after each successive exposure to the APTES solution that infiltrates the pores of the PSiM. Correspondingly, the relative intensity measured by the smartphone decreases when the spectrum redshifts due to the relative spectral positions of

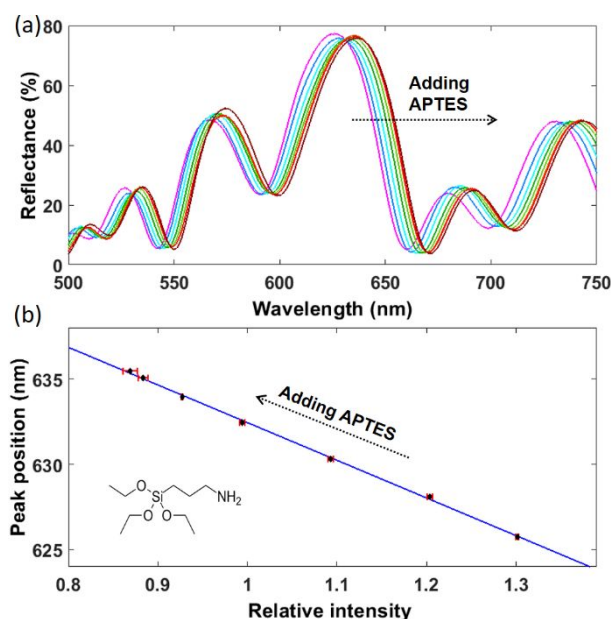


Figure 3. (a) Reflectance spectra of PSiM after adding 0.1% APTES solutions, as measured by a spectrometer. (b) Smartphone-spectrometer comparison curve that relates the longer wavelength peak position of the PSiM measured by the spectrometer and the relative intensity of light measured by the smartphone. The black diamonds are the experimental data points, the red bars show the  $\pm 3\sigma$  value from the smartphone measurements, and the blue curve is a linear fit to the black data points. Inset shows the structural formula of APTES.

the bandpass filter and resonance. Figure 3b shows the correlation between the peak wavelength measured by the spectrometer (i.e., the peak on the longer wavelength side of the microcavity resonance) and the relative intensity measured by the smartphone. A linear curve is used to fit the data with  $R^2 = 0.999$ . The error bars in the relative intensity measurements represent  $\pm 3\sigma$ , where  $\sigma$  is the standard deviation of the three relative intensity measurements taken for each APTES infiltration (details provided in S1 in ESI<sup>†</sup>). The root-mean-square deviation (RMSD) of the data points from the linear fit is used to estimate the accuracy of the PSiM-smartphone sensor. As detailed in S5 in ESI<sup>†</sup>, the RMSD = 0.11 nm, and we consider the equivalent accuracy of the smartphone measurements to be three times the RMSD (i.e., 0.33 nm). The Bland-Altman analysis shown in ESI Fig. S5<sup>†</sup>, provides further confirmation of the agreement between the smartphone and spectrometer measurements. Therefore, based on the measurements and analysis, we suggest that the PSi-smartphone sensor system could distinguish a relative intensity change that is equivalent to a microcavity spectral shift of 0.33 nm.

#### Biotin—Streptavidin sensing

To evaluate the biosensing performance of the PSiM-smartphone system, the biotin-streptavidin sensing assay was carried out. For this experiment, only the smartphone is required, but spectrometer measurements were also taken to provide further insights. Figure 4 shows the relative intensity of light measured by the smartphone as different concentrations of streptavidin molecules were exposed to the biotinylated

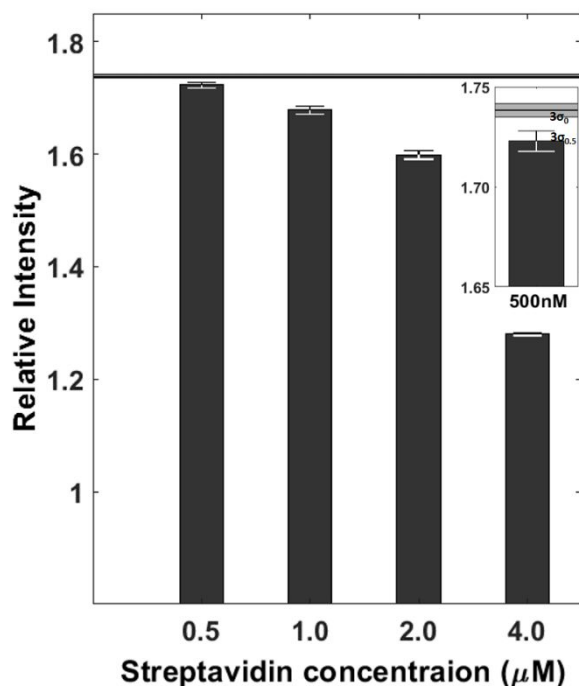


Figure 4. Relative intensity measured by smartphone when different concentrations of streptavidin are exposed to a biotin-functionalized PSiM. The detection limit is near 500 nM. Error bars represent  $\pm 3\sigma$ .

PSiM. As expected, the relative intensity decreases with increasing streptavidin concentration. We note that the change in relative intensity with respect to the streptavidin concentration is not linear across the data set because the measurements span a nonlinear region of the slope of the microcavity resonance that is probed through the bandpass filter. Figure S6 in ESI<sup>†</sup>, which shows the peak wavelength shift measured by the spectrometer as a function of streptavidin concentration, does suggest that the PSiM is being measured within the linear regime of a dose-response curve. Moreover, Fig. S6<sup>†</sup> reveals that there is minor instability of the surface functionalization of the PSiM that manifests as a slight blueshift in the spectrum when the sample is exposed to a 0 nM concentration of streptavidin (i.e., no streptavidin molecules and only solvent exposed to the sample). The biotin-streptavidin assay was repeated on three additional PSiM samples to confirm the general trend of the relative intensity measured by the smartphone upon exposure to the different streptavidin concentrations (ESI Fig. S7<sup>†</sup>). In all cases, the relative light intensity measured by the smartphone when the PSiM is exposed to 500 nM streptavidin is statistically different from the initial relative light intensity value measured before exposure to any streptavidin solutions (solid line shown in Fig. 4 and Fig. S7<sup>†</sup>). Therefore, a detection limit near 500 nM for the streptavidin molecules is estimated for the PSiM-smartphone biosensor. In order to verify that streptavidin molecules are captured selectively by biotin receptor molecules attached to the PSiM, a control experiment was carried out in which sulfo-NHS-biotin blocked streptavidin molecules were exposed to an amine-PEG-biotinylated PSiM, as described in Section 2. A blueshift was measured by the spectrometer, which we again attribute to instability of the PSiM surface modification. This

result suggests that biotin-streptavidin binding occurs specifically and, moreover, improvement in the robustness of the surface chemistry may allow even larger changes in relative intensity to be measured when a given concentration of streptavidin is exposed to a biotin-functionalized PSiM.

## 4. Conclusions

A PSi-based smartphone biosensor is demonstrated as a new sensing platform that leverages the convenience of a smartphone and the high internal active sensing surface area of a PSi film. Structural colour changes of the PSi film that result from molecules infiltrating the pores are converted to a relative intensity value by analysing the red pixel values read out from the smartphone camera image sensor. When benchmarked against a commercial spectrometer, the PSiM smartphone system exhibits an accuracy equivalent to 0.33 nm. Specific detection of streptavidin molecules was demonstrated with an estimated detection limit of 500 nM. As the PSiM biosensor supports a variety of surface functionalizations, the PSiM smartphone system could be used as a platform for the detection of a multitude of chemical and biomolecular species including DNA, small proteins, and toxins using, for example, DNA, antibody, or aptamer probes. By addressing some of the current engineering challenges and by integrating a simpler fluidic handling approach, the PSi-based smartphone biosensor has the potential for application as a POC diagnostic tool, which could be particularly useful in low-resource environments.

## Conflicts of interest

There are no conflicts to declare.

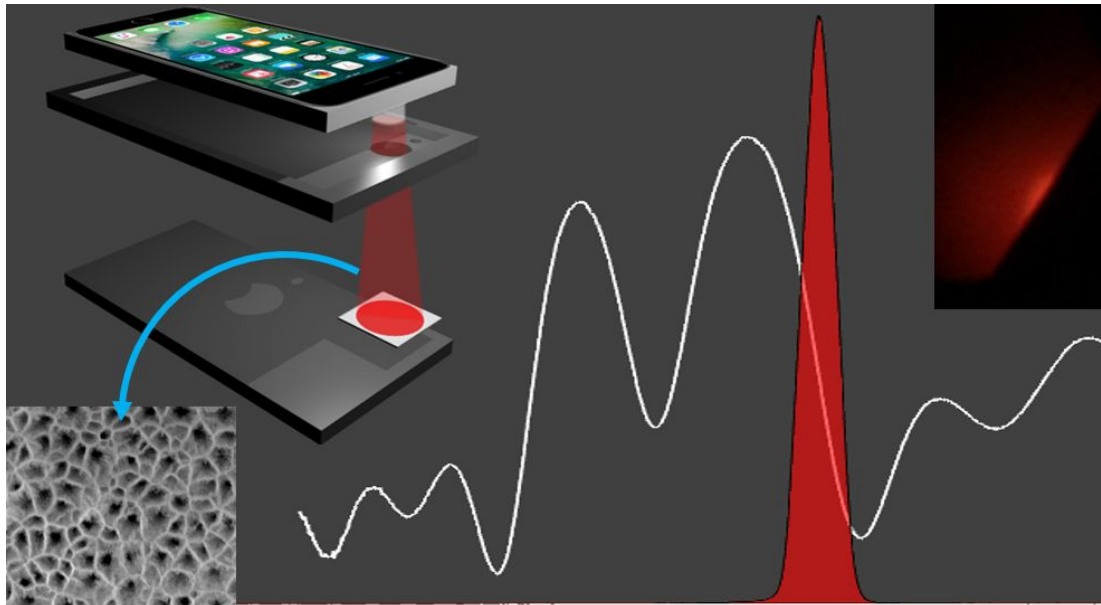
## Acknowledgement

This work was supported in part by the Army Research Office (W911NF-15-1-0176). C.A.N. acknowledges support from the NSF-REU Program (DMR-1263182). The authors would like to thank Z. Zheng and H. Yan for technical assistance with the 3D printed box and Dr. M. H. Choudhury for helpful discussions.

## Notes and references

- 1 V. Gubala, L. F. Harris, A. J. Ricco, M. X. Tan and D. E. Williams, *Anal. Chem.*, 2012, **84**, 487–515.
- 2 J. R. Crowther, *The ELISA guidebook*, Springer Science & Business Media, 2000, vol. 149.
- 3 H. Zhang, S. Wang and G. Fang, *J. Immunol. Methods*, 2011, **368**, 1–23.
- 4 K. Vekey and A. Telekes, in *Medical Applications of Mass Spectrometry*, Elsevier, 2008, pp. 7–18.
- 5 J. Homola and M. Piliarik, in *Surface plasmon resonance based sensors*, Springer, 2006, pp. 45–67.
- 6 X. D. Hoa, A. G. Kirk and M. Tabrizian, *Biosens. Bioelectron.*, 2007, **23**, 151–160.
- 7 W. M. Nelson, G. W. Long and L. M. Cockrell, in *Biological*

1	Analyst	Paper
2		
3		<i>Identification</i> , Elsevier, 2014, pp. 54–68.
4	8	D. Grieshaber, R. MacKenzie, J. Voeroes and E. Reimhult, <i>Sensors</i> , 2008, <b>8</b> , 1400–1458.
5		
6	9	F. Lisdat and D. Schäfer, <i>Anal. Bioanal. Chem.</i> , 2008, <b>391</b> ,
7		1555.
8	10	S. F. Clarke and J. R. Foster, <i>Br. J. Biomed. Sci.</i> , 2012, <b>69</b> ,
9		83–93.
10	11	J. Hu, S. Wang, L. Wang, F. Li, B. Pingguan-Murphy, T. J. Lu
11		and F. Xu, <i>Biosens. Bioelectron.</i> , 2014, <b>54</b> , 585–597.
12	12	A. K. Yetisen, M. S. Akram and C. R. Lowe, <i>Lab Chip</i> , 2013,
13		<b>13</b> , 2210–2251.
14	13	P. Abgrall and A. M. Gue, <i>J. Micromechanics</i>
15		<i>Microengineering</i> , 2007, <b>17</b> , R15.
16	14	D. Zhang and Q. Liu, <i>Biosens. Bioelectron.</i> , 2016, <b>75</b> , 273–
17		284.
18	15	D. N. Breslauer, R. N. Maamari, N. A. Switz, W. A. Lam and
19		D. A. Fletcher, <i>PLoS One</i> , 2009, <b>4</b> , 1–7.
20	16	D. Tseng, O. Mudanyali, C. Oztoprak, S. O. Isikman, I.
21		Sencan, O. Yaglidere and A. Ozcan, <i>Lab Chip</i> , 2010, <b>10</b> ,
22		1787–1792.
23	17	O. Mudanyali, S. Dimitrov, U. Sikora, S. Padmanabhan, I.
24		Navruz and A. Ozcan, <i>Lab Chip</i> , 2012, <b>12</b> , 2678–2686.
25	18	B. Y. Chang, <i>Bull. Korean Chem. Soc.</i> , 2012, <b>33</b> , 549–552.
26	19	S. Lee, S. Mehta and D. Erickson, <i>Anal. Chem.</i> , 2016, <b>88</b> ,
27		8359–8363.
28	20	M. Zangheri, L. Cevenini, L. Anfossi, C. Baggiani, P. Simoni,
29		F. Di Nardo and A. Roda, <i>Biosens. Bioelectron.</i> , 2015, <b>64</b> ,
30		63–68.
31	21	B. Berg, B. Cortazar, D. Tseng, H. Ozkan, S. Feng, Q. Wei, R.
32		Y. L. Chan, J. Burbano, Q. Farooqui, M. Lewinski, D. Di
33		Carlo, O. B. Garner and A. Ozcan, <i>ACS Nano</i> , 2015, <b>9</b> , 7857–
34		7866.
35	22	P. Preechaburana, M. C. Gonzalez, A. Suska and D. Filippini,
36		<i>Angew. Chemie - Int. Ed.</i> , 2012, <b>51</b> , 11585–11588.
37	23	Y. Liu, Q. Liu, S. Chen, F. Cheng, H. Wang and W. Peng, <i>Sci.</i>
38		<i>Rep.</i> , 2015, <b>5</b> , 1–9.
39	24	D. Gallegos, K. D. Long, H. Yu, P. P. Clark, Y. Lin, S. George,
40		P. Nath and B. T. Cunningham, <i>Lab Chip</i> , 2013, <b>13</b> , 2124.
41	25	C. Zhang, G. Cheng, P. Edwards, M.-D. Zhou, S. Zheng and
42		Z. Liu, <i>Lab Chip</i> , 2016, <b>16</b> , 246–250.
43	26	H. Yu, Y. Tan and B. T. Cunningham, <i>Anal. Chem.</i> , 2014, <b>86</b> ,
44		8805–8813.
45	27	Y. Song, W. Wei and X. Qu, <i>Adv. Mater.</i> , 2011, <b>23</b> , 4215–
46		4236.
47	28	S. K. Ramakrishan, M. Martin Fernandez, T. Cloitre, V.
48		Agarwal, F. J. G. Cuisinier and C. Gergely, <i>Sensors</i>
49		<i>Actuators, B Chem.</i> , 2018, <b>272</b> , 211–218.
50	29	A. Jane, R. Dronov, A. Hodges and N. H. Voelcker, <i>Trends</i>
51		<i>Biotechnol.</i> , 2009, <b>27</b> , 230–239.
52	30	S. Arshavsky-Graham, N. Massad-Ivanir, E. Segal and S.
53		Weiss, <i>Anal. Chem.</i> , 2019, <b>91</b> , 441–467.
54	31	M. Zhu, M. Z. Lerum and W. Chen, <i>Langmuir</i> , 2011, <b>28</b> ,
55		416–423.
56	32	Y. Zhao, G. Gaur, S. T. Retterer, P. E. Laibinis and S. M.
57		Weiss, <i>Anal. Chem.</i> , 2016, <b>88</b> , 10940–10948.
58		
59		
60		



A smartphone biosensor with minimal external components is demonstrated for highly sensitive detection of biomolecules by monitoring the structural colour of a porous silicon film.